Threshold defect production in germanium determined by density functional theory molecular dynamics simulations

E. Holmström, K. Nordlund, and A. Kuronen

University of Helsinki and Helsinki Institute of Physics, University of Helsinki, P.O. Box 64, Helsinki FIN 00014, Finland

E-mail: `eero.holmstrom@helsinki.fi`

Abstract.
We studied the threshold displacement energy in germanium using density functional theory molecular dynamics simulations. The average threshold energy over all lattice directions for creating stable Frenkel pairs was found to be $(23\pm2_{\mathrm{stat}}\pm3_{\mathrm{syst}})$ eV. In the lattice directions $\langle 111 \rangle$ and $\langle 100 \rangle$, the threshold energy was found to be $(11.5 \pm 1.5_{\mathrm{syst}})$ eV and $(19.5 \pm 1.5_{\mathrm{syst}})$ eV, respectively. In a notable fraction of all the studied directions, a bond defect was created with a lower threshold than a Frenkel pair. The average threshold energy for creating either a bond defect or a Frenkel pair was found to be $(21 \pm 1_{\mathrm{stat}} \pm 3_{\mathrm{syst}})$ eV.

1. Introduction

The threshold displacement energy E_d is the minimum amount of kinetic energy that, when released to a lattice atom in a solid, results in the formation of a stable vacancy-interstitial defect pair called a Frenkel pair [1, 2, 3]. E_d is the single most important quantity in determining primary radiation damage in any material. It can be directly used to predict the number of defects created by electron irradiation incident on a material, and in many models it is used to estimate the damage caused by high-energy ion and neutron irradiation [4, 5].

E_d is of major importance in germanium because of the extensive use of the material under irradiation. Germanium is widely used as a the bulk material of radiation detectors [6]. Additionally, the material is used increasingly in applications of solar cell technology, which often end up in space applications [7]. As a further example, the alloy SiGe has in the recent years become an important material in the manufacturing of semiconductor components [7], where ion implantation is a routinely applied method [8, 9]. In spite of this great technological interest in the quantity and extensive study on the subject, there is still considerable uncertainty in the value of E_d in germanium. Experimental values for the minimum of the threshold energy over all lattice directions range from about 15 to 30 eV [10, 11, 12, 13, 14, 15]. In particular, there is no established value for the average threshold energy over all lattice directions, $E_{d,ave}^{av}$, with values of 30 eV [16] and 18 eV[12] reported for an effective threshold energy.

In this study, we use quantum-mechanical density functional theory (DFT) [17] molecular dynamics (MD) simulations to investigate E_d in germanium. Using the DFT code SIESTA [18], we determine E_d in the principal lattice directions as well as the average threshold energy $E_{d,ave}^{av}$ over all lattice directions. DFT methods are known to generally predict irradiation-related quantities in good agreement with experiment [19, 20]. Moreover, we found in a previous study [21] that the method employed here predicted E_d in silicon in excellent agreement with experiment.

2. Method

The dynamical quantum-mechanical simulations used to determine E_d were performed using the pseudopotential, linear combination of atomic orbitals (LCAO) DFT code SIESTA as a force module to the classical MD code PARCAS [22]. However, before the simulations aimed at determining E_d were started, a thorough optimisation of the simulation parameters was performed. This was necessary for the following reason. The process of determining E_d in a specific crystallographic direction with MD simulation consists of simulating recoils of increasing energy in that direction until a permanent defect is obtained [3]. In order to find $E_{d,ave}^{av}$ within a reasonable margin of error, E_d in a number of individual uniformly randomly chosen lattice directions must be determined. Therefore, the total number of recoil simulations necessary for such a study is high. As additionally the method of DFT is computationally very heavy, it is imperative that

the simulation parameters be optimised to give as physically plausible a description of the recoil process as possible with an as computationally efficient parametrisation as possible.

2.1. Optimising the general simulation parameters

The first step in optimising the simulation parameters was to determine the smallest size of the simulation cell that would still give a reliable value for $E_{d,ave}^{av}$. For this task, to obtain an educated estimate, the well-established classical Stillinger-Weber potential [23] was used to model the Si-Si interactions. Starting from a cubic cell of 4096 atoms and ending at only 64 atoms, $E_{d,ave}^{av}$ was determined at each cell size in order to find roughly the minimum necessary size of the cell. The result was that a cell size of around 100 to 200 atoms should still give a reliable value for $E_{d,ave}^{av}$, and further experimentation with cells of also non-cubic shape resulted in a cell of 144 atoms with the z-axis of the unit cell oriented in the conventional $\langle 111 \rangle$ direction. The advantage of the geometry of the cell was that the symmetry of the diamond lattice could be exploited to study recoils in only the positive octant of the standard unit cell, which corresponded to firing recoils along the largest dimension of the 144-atom cell. This served to lessen the unphysical effects of the periodic boundaries of the cell, which were employed in all simulations throughout the work. Additionally, it was found at this stage that Berendsen temperature scaling [24] applied uniformly throughout the cell after 200 fs of the simulation had passed was a method of cooling that did not significantly affect the value of $E_{d,ave}^{av}$ as compared to using a larger cell and the physically better motivated method of cooling the cell from the borders.

Next, the simulation time was optimised in a similar fashion as the cell size. Using the 144-atom cell, $E_{d,ave}^{av}$ was determined as a function of decreasing simulation time from 9.0 to 0.5 ps. It was found that a simulation time of 3 ps should be sufficiently long for reliably labelling the formed defects stable. The results for the cell size and simulation time scaling are presented in Fig. 1. The 3 eV difference between the values of $E_{d,ave}^{av}$ obtained in the size scaling with the largest cell of 4096 atoms and the final cell of 144 atoms was used as a systematic error in all the latter results for E_d obtained within this simulation scheme.

2.2. Optimising the DFT parameters

The DFT parameters were optimised under the requirement that they yield accurate formation energies for the basic point defects while being efficient enough to enable dynamic simulations later on. The aim was to determine $E_{d,ave}^{av}$ both within the local-density approximation (LDA) and the generalised gradient approximation (GGA) for the quantum-mechanical exchange and correlation energy of DFT. The defect formation energies were considered an obvious test for the simulation scheme, as the formation energy is a fundamental and quite extensively studied quantity in describing the entities which were the very object of the work. The DFT parameters were scanned by varying
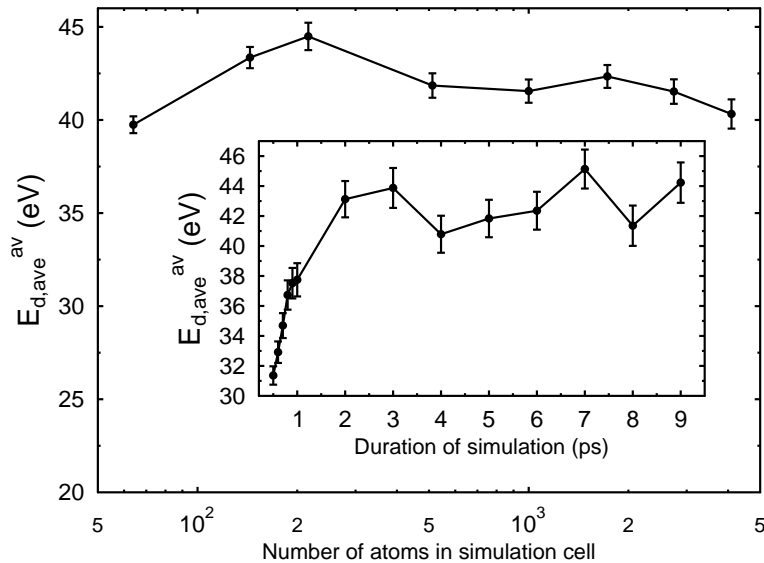
Figure 1. Scaling of the simulation cell size and simulation time with classical simulations. It was found that a cell of 100 to 200 atoms should be sufficiently large for a reliable determination of $E_{d,ave}^{av}$, and the settled size of the cell became 144 atoms. Using this simulation cell, it was found that a duration of 3 ps for the simulation is sufficiently long for reliably labelling the formed defects stable.

the LCAO basis set, the k-point sampling of the Brillouin zone, and the equivalent plane-wave cutoff energy. The basis was varied between single-zeta and double-zeta and each with polarisation orbitals included. The number of k-points was varied between only the Γ point, 4, and 18 points for the LDA scheme, and for the GGA scheme the variation was between the Γ point, 2, and 12 k-points. The equivalent plane wave cutoff energy was varied between 100.0 and 300.0 Ry.

The defect formation energy is defined as [25]

$$E^f = \left(\frac{E_d}{N_d} - \frac{E_u}{N_u}\right)N_d, \tag{1}$$

where E_d and N_d are the potential energy and number of atoms in the cell with the defect, and E_u and N_u are the corresponding quantities in a defect-free cell. The studied point defects were the $\langle 110 \rangle$ split or dumbbell interstitial, the hexagonal interstitial, the tetrahedral interstitial, the monovacancy, the ground state Frenkel pair which was found to have a tetrahedral interstitial, and the bond defect [26, 27, 28]. For each of these cases, the structure of the defect was relaxed via full conjugate gradient optimisation. During these static calculations it became clear, that in both the LDA and GGA schemes only a single-zeta basis set would be computationally feasible in the upcoming dynamical simulations. Finally, three such single-zeta sets, one within the LDA and two within the GGA schemes, were settled upon. Four k-points in a Monkhorst-Pack grid [29],

a cutoff energy of 100.0 Ry, and the Ceperley-Alder exchange-correlation funtional as parametrised by Perdew and Zunger [30] were used for the LDA set. The first GGA set in turn consisted of 2 k-points, a cutoff energy of 100.0 Ry, and the Perdew-Burke-Ernzerhof exchange-correlation functional [31]. The second GGA set included 12 k-points instead of two. The latter two parameter sets shall henceforth be denoted GGA I and GGA II, respectively.

The formation energies of the interstitial and vacancy defects are shown in Tables 1 and 2 for both the LDA and GGA parameter sets as a function of the k-point sampling. It can be seen from these results that the parameter sets chosen for the dynamical runs are sufficiently converged with respect to the k-point sampling. The formation energies were also found to be well converged in terms of the equivalent plane-wave cutoff energy. However, the hexagonal interstitial was not stable with respect to conjugate gradient relaxation within either the LDA or GGA parameter sets. This is most likely due to the limitations of the single-zeta basis, but was not considered a fatal shortcoming provided the other point defects could be described with satisfactory accuracy. The results for all the studied defects within the chosen LDA and GGA schemes as well as results from previous studies are shown in Table 3. It can be seen here that our results are quite well in line with previous, albeit more precise LDA DFT calculations. As a final separate test for the DFT scheme, the energy of the germanium dimer was calculated at distances of $r = 0.8$ to $10\mathring{A}$ and compared to an all-electron calculation [32]. It was found that reliable calculations could be performed within our LDA and GGA schemes up to recoil energies of at least 50 eV, which was estimated to be higher than E_d by a safe margin in most lattice directions.

Table 1. Formation energies of the basic point defects in eV calculated within the LDA scheme (see text) as a function of the number of k-points used in sampling the BZ.

No. of k-points	Split-$\langle 110 \rangle$	Tetrahedral	Vacancy
Γ	2.7	2.5	1.6
4	3.6	4.1	2.5
18	3.6	3.8	2.5

Table 2. Formation energies of the basic point defects in eV calculated within the GGA scheme (see text) as a function of the number of k-points used in sampling the BZ.

No. of k-points	Split-$\langle 110 \rangle$	Tetrahedral	Vacancy
Γ	2.4	2.1	1.4
2	3.2	3.0	2.0
12	3.1	3.1	2.3

Table 3. Formation energies of the basic point defects in eV calculated within the LDA and GGA schemes, and results from other DFT studies. The Frenkel pair for our calculations consists of a tetrahedral interstitial and a vacancy with a distance of 4.9 Å between them. No formation energy for a Frenkel pair was found in the literature.

Defect	LDA	GGA I	GGA II	Other studies
Split-$\langle 110 \rangle$	3.6	3.2	3.1	2.3[33], 3.6[34]
Tetrahedral	4.1	3.0	3.1	3.2[33], 3.9[34]
Vacancy	2.5	2.0	2.3	2.0[35]
Frenkel pair	4.9	4.2	4.2	-
Bond defect	2.5	2.4	2.4	2.8[34]

2.3. Dynamical simulations

After the optimisation of the simulation scheme, the MD runs aimed at determining $E_{d,ave}^{av}$ were performed. E_d was determined in 80 random directions within the LDA and GGA I schemes and in 20 random directions within the GGA II scheme. In addition, E_d was determined for the low-index lattice directions $\langle 111 \rangle$ and $\langle 100 \rangle$.

3. Results

The results of the dynamical simulations for determining E_d are presented in Table 4. As was the case in our previous study with silicon [21], a fourfold-coordinated bond defect was observed in many of the end states of the recoil simulations. Hence, in addition to the average threshold energy for producing a Frenkel pair $E_{d,ave}^{av,FP}$, we present the average threshold energy for producing either a Frenkel pair or a bond defect, $E_{d,ave}^{av,BD/FP}$. The results for the direction-specific thresholds are those for creating Frenkel pairs, which turned out lower than the thresholds for creating bond defects in those directions. A bond defect was created with a lower threshold energy than a Frenkel pair in some 40% of the studied directions within the LDA scheme, some 20% of the directions within the GGA I scheme, and 10% of the directions within GGA II. A vast majority of all Frenkel pair end states, about 90% within LDA and GGA I and 95% within GGA II, consisted of a tetrahedral interstitial and a monovacancy, with the dumbbell interstitial replacing the tetrahedral one in the remaining cases.

4. Discussion

It can be seen from Table 4 that the results for $E_{d,ave}^{av,FP}$ from the GGA I and GGA II schemes are within error margins of each other, but that the LDA result is somewhat higher. As the LDA and GGA I calculations for $E_{d,ave}^{av,FP}$ were both performed with 80 random directions and the GGA II result with 20 directions, the GGA I result of $(23 \pm 2_{\mathrm{stat}} \pm 3_{\mathrm{syst}})$ eV is to be considered the most reliable value for $E_{d,ave}^{av,FP}$ of the three, with GGA II serving as a confirmation for its reliability. The same reasoning

Table 4. Threshold displacement energies in eV as determined within the LDA and GGA schemes. The energy step size was 1 eV for the direction-specific thresholds, implying an error of ± 0.5 eV in addition to the systematic error of ± 1.0 eV resulting from the scaling of the cell size. For the averages, a systematic error of ± 3 eV due to the scaling of the cell size and the standard error of the mean are reported. A and B denote the closed and open $\langle 111 \rangle$ directions, respectively.

	LDA	GGA I	GGA II
$\langle 111 \rangle (A)$	$12.5 \pm 1.5_{\text{syst}}$	$12.5 \pm 1.5_{\text{syst}}$	$12.5 \pm 1.5_{\text{syst}}$
$\langle 111 \rangle (B)$	$10.5 \pm 1.5_{\text{syst}}$	$11.5 \pm 1.5_{\text{syst}}$	$11.5 \pm 1.5_{\text{syst}}$
$\langle 100 \rangle$	$18.5 \pm 1.5_{\text{syst}}$	$19.5 \pm 1.5_{\text{syst}}$	$19.5 \pm 1.5_{\text{syst}}$
$E_{d,ave}^{av,FP}$	$27 \pm 1_{\text{stat}} \pm 3_{\text{syst}}$	$23 \pm 2_{\text{stat}} \pm 3_{\text{syst}}$	$20 \pm 2_{\text{stat}} \pm 3_{\text{syst}}$
$E_{d,ave}^{av,BD/FP}$	$22 \pm 1_{\text{stat}} \pm 3_{\text{syst}}$	$21 \pm 1_{\text{stat}} \pm 3_{\text{syst}}$	$19 \pm 2_{\text{stat}} \pm 3_{\text{syst}}$

applies to $E_{d,ave}^{av,FP/BD}$. The value of 23 eV for $E_{d,ave}^{av,FP}$ is situated roughly halfway between the existing experimental values for an average threshold displacement energy in germanium. The two experimental values of 18[12] and 30 eV [16] are not, however, direct determinations of the average threshold over all lattice directions and are hence more suitably called effective thresholds.

As for the directional thresholds, no lower threshold was found in each simulation scheme than the threshold energy in the direction $\langle 111 \rangle (B)$, which is therefore the global minimum of E_d within this study. A comparison to experiment for this threshold energy is possible, as several determinations for the onset of radiation damage in germanium have been performed [10, 11, 12, 13, 14, 15]. The experimental values are mostly around 15 eV, which is slightly higher than the values of $(10.5 \pm 1.5_{\text{syst}})$ eV and $(11.5 \pm 1.5_{\text{syst}})$ eV in the LDA and GGA schemes, respectively. Here the GGA I and GGA II results in particular are quite close to experiment, which lends reliability to the determined value of 23 eV for $E_{d,ave}^{av,FP}$.

That the tetrahedral interstitial dominates in the end state Frenkel pairs over the split interstitial is in agreement with our result that the ground state Frenkel pair comprises a tetrahedral interstitial and a monovacancy. The notable amount of bond defects observed throughout the simulations serves to indicate that this relatively new form of point defect may play a significant role in the primary radiation damage of germanium. The results are in this respect similar to those found in the case of silicon [21].

5. Conclusions

The threshold displacement energy in germanium was studied using quantum-mechanical density functional theory molecular dynamics simulations. A value of $(23 \pm 2_{\text{stat}} \pm 3_{\text{syst}})$ eV was found for the average threshold energy for producing a Frenkel pair over all lattice directions, and a global minimum of $(11.5 \pm 1.5_{\text{syst}})$ eV was determined for the threshold, in fair agreement with experiment. A large amount

of fourfold-coordinated bond defects were observed in the end states of the simulations, and hence a threshold energy of $(21\pm1_{\mathrm{stat}}\pm3_{\mathrm{syst}})$ eV for producing either a Frenkel pair or a bond defect was also calculated. The end state interstitial type was overwhelmingly dominated by the tetrahedral interstitial, which constitutes the interstitial in the ground state Frenkel pair.

References

[1] Lucasson P 1975 *Fundamental Aspects of Radiation Damage in Metals* ed Robinson M T and Young Jr F N (Springfield: ORNL) pp 42–65

[2] Jung P 1991 (*Landolt-Brnstein, New Series III* vol 25) ed Ullmaier H (Berlin: Springer) chap 1, pp 1–86

[3] Nordlund K, Wallenius J and Malerba L 2005 *Nucl. Instr. Meth. Phys. Res. B* **246** 322–332

[4] Kinchin G and Pease R 1955 *Rep. Prog. Phys.* **18** 1

[5] Biersack J P and Haggmark L G 1980 *Nucl. Instr. Meth.* **174** 257

[6] Lutz G 2007 *Semiconductor Radiation Detectors – Device Physics* (Springer-Verlag, Berlin)

[7] U.S. Department of the Interior: U.S. Geological Survey, Mineral Commodity Summaries, January 2009

[8] Gibbons J F 1968 *Proceedings of the IEEE* **56** 295–319

[9] Mayer J W, Eriksson L and Davies J A 1970 *Ion Implantation in Semiconductors: Silicon and Germanium* (Academic Press, Inc.)

[10] Klontz E E and Lark-Horovitz K 1951 *Phys. Rev.* **82** 763

[11] Vavilov, Smirnov, Galkin, Spitsyn and Patskevich 1957 *Sov. Phys. (Tech. Phys.)* **1** 1805

[12] Loferski J and Rappaport P 1958 *Phys. Rev.* **111** 432

[13] Smirnov L S and Glazunov P A 1960 *Sov. Phys. (Sol. State)* **1** 1262

[14] Brown W L and Augustyniak W M 1959 *J. Appl. Phys.* **30** 1300

[15] Poulin F and Bourgoin J 1980 *Rev. Phys. Appl.* **15** 15

[16] Vitovskii N A, Mustafakulov D and Chekmareva A P 1977 *Fiz. Tekh. Poluprovodn.* **11** 1747

[17] For a review, see R. O. Jones and O. Gunnarsson, Rev. Mod. Phys. **61**, 689 (1989)

[18] Sole J M, Artacho E, Gale J D, Garca A, Junquera J, Ordejn P and Snchez-Portal D 2002 *J. Phys.: Condens. Matter* **14** 2745

[19] Sadigh B, Lenosky T J, Theiss S K, Caturla M J, Diaz de la Rubia T and Foad M A 1999 *Phys. Rev. Lett.* **83** 4341

[20] Fu C C, Torre J D, Willaime F and Bocquet J L 2005 *Nature Materials* **4** 68–74

[21] Holmstrm E, Kuronen A and Nordlund K 2008 *Phys. Rev. B* **78** 045202

[22] Nordlund K 2006 PARCAS computer code. The main principles of the molecular dynamics algorithms are presented in [36, 37]. The adaptive time step and electronic stopping algorithms are the same as in [38]

[23] Stillinger F A and Weber T A 1985 *Phys. Rev. B* **31** 5262

[24] Berendsen H J C, Postma J P M, van Gunsteren W F, DiNola A and Haak J R 1984 *J. Chem. Phys.* **81** 3684

[25] Qian G X, Martin R M and Chadi D J 1988 *Phys. Rev. B* **38** 7849

[26] Tang M, Colombo L, Zhu J and Diaz de la Rubia T 1997 *Phys. Rev. B* **55** 14279

[27] Cargnoni F, Gatti C and Colombo L 1998 *Phys. Rev. B* **57** 170

[28] Goedecker S, Deutsch T and Billard L 2002 *Phys. Rev. Lett.* **88** 235501

[29] Monkhorst H J and Pack J D 1976 *Phys. Rev. B* **13** 5188

[30] Perdew J P and Zunger A 1981 *Phys. Rev. B* **23** 5075

[31] Perdew J P, Burke K and Ernzerhof M 1996 *Phys. Rev. Lett.* **77** 3865

[32] DMol is a trademark of AccelRys. Inc.

[33] da Silva A J R, Janotti A and Fazzio A 2000 *Phys. Rev. B* **62** 9903

[34] Moreira M D and Miwa R H 2004 *Phys. Rev. B* **70** 115215
[35] Fazzio A, Janotti A and da Silva A J R 2000 *Phys. Rev. B* **61** R2401
[36] Nordlund K, Ghaly M, Averback R S, Caturla M, Diaz de la Rubia T and Tarus J 1998 *Phys. Rev. B* **57** 7556–7570
[37] Ghaly M, Nordlund K and Averback R S 1999 *Phil. Mag. A* **79** 795
[38] Nordlund K 1995 *Comput. Mater. Sci.* **3** 448